INTERNATIONAL JOURNAL FOR NUMERICAL METHODS IN FLUIDS
Int. J. Numer. Meth. Fluids **28**: 601–616 (1998)

SIMULATION OF VORTEX SHEDDING PAST A SQUARE CYLINDER WITH DIFFERENT TURBULENCE MODELS

G. BOSCH[1] AND W. RODI*

Institute for Hydromechanics, University of Karlsruhe, Karlsruhe, Germany

SUMMARY

This paper presents the results of numerical simulations of vortex shedding past a free-standing square cylinder at $Re_D = 22000$, obtained with different turbulence models. Using wall functions, the standard k–ε model is compared with a modification suggested by Kato and Launder (*Proc. 9th Symp. Turbulent Shear Flows*, Kyoto, 10-4-1 (1993)). In addition, both versions are used in a two-layer approach, in which the flow close to the cylinder is computed with a locally more suitable one-equation turbulence model and only outside the viscous near-wall layer with the two mentioned high-Re model versions. To allow a comparison, the simulations are performed first using the same computational domain and boundary conditions as in previous investigations. Then results are presented that were obtained on a computational domain and with boundary conditions more suitable for a comparison with the experiments.

KEY WORDS: turbulence modeling; CFD; finite volume method; vortex shedding; two-layer approach

1. INTRODUCTION

Vortex shedding is an unsteady flow phenomenon which occurs frequently behind relatively slender, bluff structures, called cylinders in the present study, and is therefore of great practical importance. At relatively small Reynolds numbers $Re_D = u_\infty D/\nu$ based on the diameter D of the cylinder, numerical simulations carried out by solving the two-dimensional unsteady Navier–Stokes equations were quite successful. At high Reynolds numbers, which are more relevant in practice, three-dimensional stochastic turbulent fluctuations Φ' are superimposed on the periodic unsteady motion $\langle\Phi(t)\rangle$ of the vortex shedding, as illustrated in Figure 1. If a sensor, such as a hot-film device, is placed in the wake of a bluff body experiencing vortex shedding, a signal $\Phi(t)$ as shown in Figure 1 will be detected with a periodic component of the vortex-shedding period T_P and a characteristic time scale T_t of the turbulent fluctuations. This superimposed stochastic turbulent motion cannot yet be resolved by a direct numerical simulation. Large eddy simulations are possible in which the low frequency part of the stochastic motion is calculated directly, while the unresolved high frequency part is simulated with a subgrid scale model. Such large eddy simulations are, however, very expensive. The present paper is concerned with the use of statistical turbulence models, in which the complete

* Correspondence to: Institute for Hydromechanics, University of Karlsruhe, Karlsruhe D-76128, Kaierstrasse 12, Germany.
[1] Present address: Laboratoire de Mécanique des Fluides, URA CNRS 1217, Ecole Centrale de Nantes, 1 rue de la Noë, BP 92101, F-44321 Nantes Cedex 03, France.

CCC 0271–2091/98/140601–16$17.50

Received May 1997
Revised October 1997

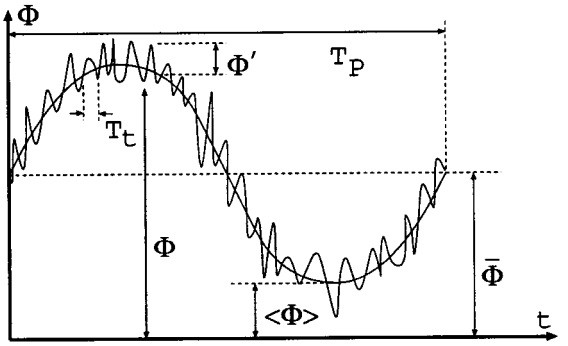

Figure 1. Triple decomposition of a turbulent, unsteady signal.

spectrum of the stochastic motion must be simulated by the turbulence model. To this end, the instantaneous flow quantities $\Phi(t)$, such as the components $v_i(t)$ or the pressure $p(t)$, are separated into a time mean component $\bar{\Phi}$, a periodic component $\tilde{\Phi}(t)$ and the turbulent fluctuating component Φ':

$$\Phi(t) = \bar{\Phi} + \tilde{\Phi}(t) + \Phi' = \langle\Phi\rangle(t) + \Phi'. \tag{1}$$

Together, the time mean and the periodic part are called the phase-averaged or ensemble-averaged component $\langle\Phi\rangle(t)$, which is resolved in the numerical calculation.

The LDA measurements by Lyn *et al.* [2] of vortex-shedding flow past a square cylinder at $Re_D = 22000$ have become a standard test case for unsteady turbulent flow of this kind (see References [3,4]) because in these measurements, the triple decomposition introduced above was performed in the data reduction so that phase-averaged quantities were obtained. Therefore, these measurements allow insight into the complex interaction between the different scales of motion. Franke [5]—see also Franke and Rodi [6]—was the first to present results of numerical predictions for this flow by solving the ensemble-averaged two-dimensional equations, using both the standard k–ε model and the full Reynolds stress model of Launder *et al.* [7], both with wall functions and in a two-layer approach. In the meantime, other calculations for the same flow have been obtained with various statistical models (see e.g. References [1,8]). These agree only partly with Franke's results, and modifications to the k–ε model were proposed to improve the predictions. Large eddy simulations have in the meantime also been carried out (see e.g. References [9,10]).

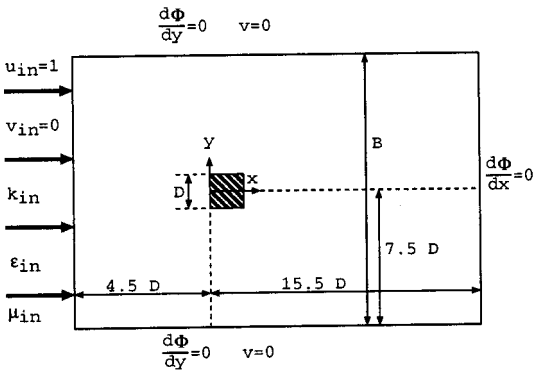

Figure 2. Computational domain and boundary conditions chosen by Franke [4].

Franke and Rodi [6] have shown that the occurrence and quality of the vortex-shedding prediction depend strongly on the turbulence model used. The standard k–ε model was found to severely underpredict the strength of the shedding motion, mainly because of excessive production of turbulent kinetic energy in the stagnation region in front of the cylinder. Reynolds stress models avoid this problem, as does the modification of the k–ε model proposed by Kato and Launder [1]. In addition, the computational domain and the inlet conditions chosen by Franke and used in most of the other studies were found to be inappropriate for the simulation of the flow investigated experimentally by Lyn *et al.* (see Bosch [11]).

In this paper, new calculations of the case studied by Lyn *et al.* will be presented, in which the results obtained with the modification of Kato and Launder are compared with those obtained with the standard k–ε model, combining both models with either wall functions or in a two-layer approach with the one-equation model of Norris and Reynolds [12]. For a comparison with previous results, the computation domain and boundary conditions chosen by Franke [5] will be used. Results obtained with optimized calculation domain and boundary conditions will also be included in order to provide a new frame of reference.

2. MATHEMATICAL MODEL

2.1. Numerical procedure

The two-dimensional ensemble-averaged unsteady Navier–Stokes equations, together with the continuity equation, are solved numerically with the iterative finite volume method FAST-2D, the basic features of which are described by Majumdar *et al.* [13]. This is a general purpose code for analyzing fluid flow. The method uses a non-staggered grid and Cartesian velocity components, handles the pressure–velocity coupling with the SIMPLEC algorithm [14], employs the special momentum interpolation method of Rhie and Chow [15] needed for the non-staggered variable arrangement, and solves the resulting system of algebraic equations iteratively with the TDMA (see e.g. Reference [16]).

For spatial discretization, the Quick convection scheme of Leonard [17] was used. The Quick scheme combines the high accuracy of a third-order scheme with the stabilizing effect of upwind weighting. A disadvantage is its unboundedness, which may cause over- and undershoots. Therefore, the Quick scheme is not suitable for the transport equations of turbulence models and the Hybrid central upwind scheme, described by Patankar [18], is used for $\langle k \rangle$ and $\langle \varepsilon \rangle$. The results obtained with the Quick scheme using the 'optimized mesh' have been compared with simulations using the HLPA scheme of Zhu [19], which is suitable for all the transport equations. No difference was found and the solutions are also grid-independent. When the Hybrid scheme was applied to all equations, a steady flow was obtained, because this scheme introduces too much numerical diffusion.

For time discretization, the fully implicit scheme (FI) was used, which is a backward difference approximation of the unsteady terms and has an approximation error of second-order, thus contributing to the numerical diffusion. Bosch [11] has shown, that for the used time step of $\Delta t^* = 0.02$ (the non-dimensional time scale is defined as $t^* = tu_\infty/D$) this scheme is sufficient.

2.2. Turbulence modeling

The Reynolds stresses $\langle u_i' u_j' \rangle$ appearing in the ensemble-averaged Navier–Stokes equations are determined by a turbulence model. The *Standard k–ε model of Launder and Spalding* [20] uses the eddy viscosity concept of Boussinesq:

$$\langle u_i' u_j' \rangle = \nu_t \left(\frac{\partial \langle u_i \rangle}{\partial x_j} + \frac{\partial \langle u_j \rangle}{\partial x_i} \right) - \frac{2}{3} \langle k \rangle \, \delta_{ij}. \tag{2}$$

This concept works on the assumption that the Reynolds stresses are proportional to the local ensemble-averaged velocity gradients and that the proportionality factor, the eddy viscosity ν_t, is a scalar quantity. In the k–ε model the eddy viscosity is related to the turbulent kinetic energy $\langle k \rangle$ and to the rate of its dissipation $\langle \varepsilon \rangle$:

$$\nu_t = c_\mu \frac{\langle k \rangle^2}{\langle \varepsilon \rangle}. \tag{3}$$

The spatial and temporal distribution of $\langle k \rangle$ and $\langle \varepsilon \rangle$ is determined from differential transport equations for these quantities, considering the history and transport effects of turbulence (see e.g. Reference [21]):

$$\frac{\partial \langle k \rangle}{\partial t} + \frac{\partial [\langle u_l \rangle \langle k \rangle]}{\partial x_l} = \frac{\partial}{\partial x_l} \left(\left(\nu + \frac{\langle \nu_t \rangle}{\sigma_k} \right) \frac{\partial \langle k \rangle}{\partial x_l} \right) + P_k - \langle \varepsilon \rangle, \tag{4}$$

$$\frac{\partial \langle \varepsilon \rangle}{\partial t} + \frac{\partial [\langle u_l \rangle \langle \varepsilon \rangle]}{\partial x_l} = \frac{\partial}{\partial x_l} \left(\left(\nu + \frac{\langle \nu_t \rangle}{\sigma_\varepsilon} \right) \frac{\partial \langle \varepsilon \rangle}{\partial x_l} \right) + C_{\varepsilon 1} P_k \frac{\langle \varepsilon \rangle}{\langle k \rangle} - C_{\varepsilon 2} \frac{\langle \varepsilon \rangle^2}{\langle k \rangle}, \tag{5}$$

with

$$P_k = c_\mu \langle \varepsilon \rangle S^2 \quad \text{and} \quad S = \frac{\langle k \rangle}{\langle \varepsilon \rangle} \sqrt{\frac{1}{2} \left[\frac{\partial \langle u_i \rangle}{\partial x_j} + \frac{\partial \langle u_j \rangle}{\partial x_i} \right]^2}.$$

S is the symmetric deformation of the fluid. The values of the k–ε model constants are: $c_\mu = 0.09$, $C_{\varepsilon 1} = 1.44$, $C_{\varepsilon 2} = 1.92$, $\sigma_k = 1.0$ and $\sigma_\varepsilon = 1.3$.

The modification of Kato and Launder [1] was developed to cure the overproduction of the turbulent kinetic energy in stagnation regions (see Reference [22]). In these regions, shear stress production of k is small and normal stress production dominates. With an isotropic eddy viscosity, as used in the standard k–ε model, the normal stresses cannot be predicted correctly, leading to the observed excessive production. On the stagnation streamline the (normal stress) production of k is $P_{k,c} = -[\langle u'^2 \rangle - \langle v'^2 \rangle](\partial \langle u \rangle / \partial x)$, which leads to $P_{k,k\varepsilon} = 4 \langle \nu_t \rangle (\partial \langle u \rangle / \partial x)^2$, when the normal stresses $\langle u'^2 \rangle$ and $\langle v'^2 \rangle$ are determined by the isotropic eddy viscosity relation.

Bypassing the eddy viscosity relation (2) for the stresses, Kato and Launder introduced the following ad-hoc model relation for the production of $\langle k \rangle$:

$$P_k = c_\mu \langle \varepsilon \rangle S \Omega \quad \text{and} \quad \Omega = \frac{\langle k \rangle}{\langle \varepsilon \rangle} \sqrt{\frac{1}{2} \left[\frac{\partial \langle u_i \rangle}{\partial x_j} - \frac{\partial \langle u_j \rangle}{\partial x_i} \right]^2}. \tag{6}$$

The quantity Ω is a rotation parameter and is proportional to the magnitude of the local vorticity. The flow does not have any vorticity on the stagnation streamline, so that Ω vanishes there. On the other hand, in simple shear layers the production terms of the standard k–ε model and the modification of Kato and Launder are identical and thus the constants of the k–ε model do not need to be recalibrated for this modification. The modification of Kato and Launder is suitable for general flow configurations involving stagnation regions, not only for vortex-shedding flows.

High Reynolds number models, such as the standard $k-\varepsilon$ model and the Kato–Launder modification, are not suitable for the flow close to walls. The viscosity-affected region close to walls can be bridged either by wall functions (see Reference [20]) or calculated using a two-layer approach, resolving the viscosity-affected region by using a locally more suitable one-equation model.

The one-equation model of Norris and Reynolds [12] was employed, which solves only the transport equation for the ensemble-averaged turbulent kinetic energy $\langle k \rangle$. Instead of determining $\langle \varepsilon \rangle$ from a transport equation, the turbulent length scale L_t, whose behaviour is well known near walls, is prescribed. The dissipation $\langle \varepsilon \rangle$ is then determined from the calculated value of $\langle k \rangle$ and the length scale. The model equations read:

$$\langle \nu_t \rangle = f_\mu c_\mu^* \sqrt{\langle k \rangle} L_t, \tag{7}$$

$$f_\mu = 1 - \exp(-A_\mu Re_y) \quad \text{with:} \quad Re_y = \frac{\sqrt{\langle k \rangle} y_n}{\nu}, \tag{8}$$

$$L_t = c_{NR} \kappa y_n, \tag{9}$$

$$\langle \varepsilon \rangle = \frac{\langle k \rangle^{3/2}}{L_t} \left(1 + \frac{\nu c_\varepsilon}{\sqrt{\langle k \rangle} L_t} \right). \tag{10}$$

The constants of the one-equation model are: $A_\mu = 0.0198$, $c_\mu^* = 0.084$, $c_{NR} = 6.41$ and $c_\varepsilon = 13.2$. κ is the Van Kármán constant with the value $\kappa = 0.4187$. According to the suggestions of Cordes [23] for the two-layer approach, the one-equation model and the high-*Re* model to be used away from the wall are matched where $f_\mu = 0.95$.

2.3. Computational domain and boundary conditions

In this section, the computational domain and the boundary conditions are summarized. Three different types of computational meshes will be used, namely Frankes' mesh, the 'optimized' mesh and a mesh suitable for the two-layer approach. Figure 2 shows the computational domain and the boundary conditions used by Franke. The inlet of the computational domain is located at $x/D = -4.5$ (the co-ordinate system has its origin in the center of the front face of the cylinder). At this boundary inlet, conditions are specified with constant values for the velocities $\langle \vec{v} \rangle = (u_\infty, 0)$ and the turbulence quantities $\langle k \rangle$ and $\langle \varepsilon \rangle$. The level of $\langle k \rangle$ was chosen to match the turbulence levels $Tu = \sqrt{u'^2} = 2\%$ measured by Lyn *et al.*

The level of the dissipation rate $\langle \varepsilon \rangle$ at the inlet of the computational domain is not known from the experiments, but needs to be specified as a boundary condition for solving the transport equation of $\langle \varepsilon \rangle$. Because of this, the value of $\langle \varepsilon \rangle$ at the inlet is computed from Equation (3) by specifying the ratio $r_\mu = \nu_t / \nu$. Franke chose the value $r_\mu = 100$, which is in the commonly accepted range used with the $k-\varepsilon$ model, if no other information is available.

The width B of the computational domain is chosen to be $15D$, which gives a blockage $D/B = 6.6\%$, which is slightly smaller than in the experiments of Lyn *et al.* ($D/B = 7\%$). The channel walls are approximated in the numerical simulations by a symmetry plane with all the gradients normal to the boundary $\partial \langle \Phi \rangle / \partial y$ and the normal velocity $\langle v \rangle$ vanishing. At the outlet computational domain, a zero streamwise gradient is specified with $\partial \langle \Phi \rangle / \partial x$, which implies that $\langle v \rangle$ vanishes because of the continuity equation. Franke placed the outlet condition at $x/D = 15.5$ downstream of the cylinder.

The computational mesh suitable for calculations with wall functions is shown in Figure 3 and has 70×63 cells. Near the walls of the cylinder the width of the first cell, was chosen as $y_w/D = 0.022$.

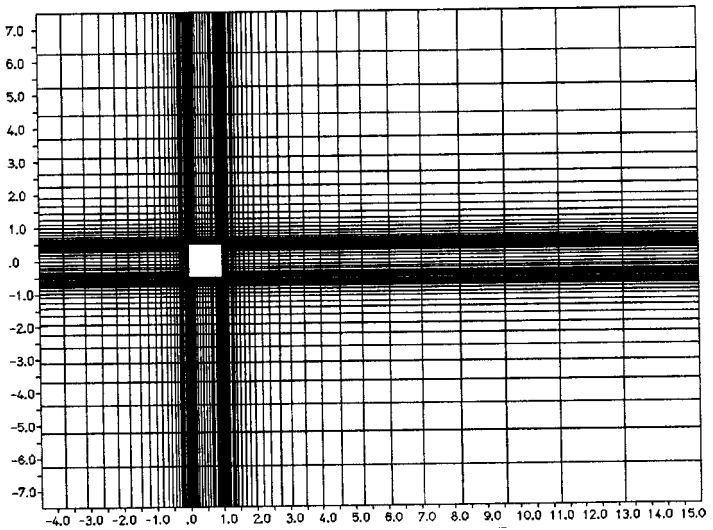

Figure 3. Computational mesh.

The distance of the grid lines is in accordance with a geometric series, with a stretching ratio of $q_x = \Delta x_i / \Delta x_{i-1} = 0.838$ in front of, $q_x = 1.173$ and $q_x = 0.853$ along the sides, and $q_x = 1.188$ behind the cylinder in the x-direction. In the y-direction the mesh is symmetric with respect to $y = 0$ and the stretching ratio below the cylinder is $q_y = \Delta y_i / \Delta y_{i-1}$, and along the cylinder $q_y = 1.221$.

In this paper, results with the so called 'optimized' computational mesh (see References [11,24]) are also presented. This mesh is shown in Figure 4 and has 99×75 cells. The inlet location is now at $x/D = -10$, because it was found that at $x/D = -4.5$, where the inlet was specified in the original computational domain of Franke, the velocity and pressure are already

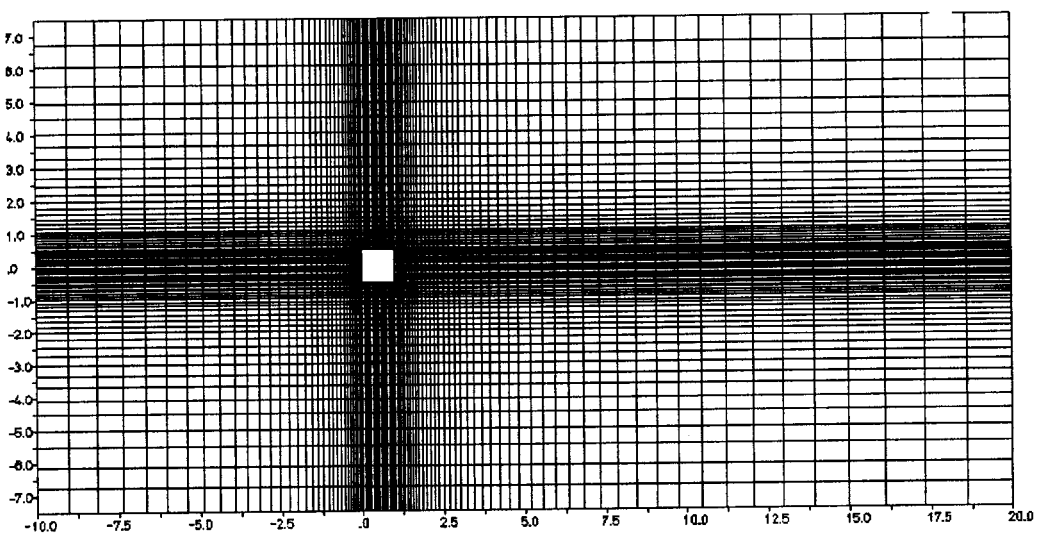

Figure 4. Optimized computational mesh.

Table I. Force coefficients and Strouhal number in comparison with other numerical studies

Author		Turbulence model	$\overline{c_D}$	c'_D	c'_L	*Str*
Kato and Launder	WF	Standard $k-\varepsilon$ model	1.660	–	0.100	0.127
present	WF	Standard $k-\varepsilon$ model	1.618	0.0003	0.050	0.126
Kato and Launder	WF	Modification of Kato and Launder	2.050	0.0212	0.820	0.145
present	WF	Modification of Kato and Launder	2.108	0.0325	1.012	0.146
Franke present	TL	Standard $k-\varepsilon$ model	1.790	0.0000	0.228	0.124
	TL	Standard $k-\varepsilon$ model	1.750	0.0012	0.178	0.122

disturbed by the presence of the cylinder. In addition, the outlet condition is specified further downstream, now at $x/D = 20$, in order to reduce its influence on the flow close to the cylinder.

The maximum stretching of successive mesh cells is limited to $0.9 \leq q_x, q_y \leq 1.1$, which gives a much smoother variation. The width of the first cells adjacent to the cylinder is $y_w/D = 0.05$. The results obtained with this mesh have been compared with results obtained with meshes having 109×85 and 143×108 cells and no change was observed.

When the two-layer approach is used, the viscous sublayer close to the cylinder needs to be resolved by the computational mesh and a value of $y^+ \approx 1$ is required for the first computational point close to the cylinder. Therefore, the width of the first cell was reduced to a value of $y_w/D = 0.005$ (146×127 computational cells) and $y_w/D = 0.002$ (169×169 computational cells), when the inlet is located at $x/D = -10$ and the outlet at $x/D = 20$, and to $y_w/D = 0.001$ with 169×169 computational cells, if the inlet is located at $x/D = -4.5$ and the outlet at $x/D = 15.5$. With the improved boundary conditions, no significant influence on the force coefficients or the Strouhal numbers could be found with respect to the mesh refinement.

The boundary condition for the dissipation rate $\langle \varepsilon \rangle$ at the inlet of the computational domain has a strong influence on the results. Some simulations were performed with $r_\mu = 100$ for comparison with previous numerical results obtained with this value. According to estimations of the turbulent length scale of the oncoming flow [11,24], a value of $r_\mu = 10$ corresponds better to the experiments of Lyn *et al.* [2] and so this new value is used in combination with the optimized mesh.

3. RESULTS

3.1. Comparison with previous numerical results

For a comparison of the present results with previous results, the same calculation domain and mesh were used and the same boundary conditions specified, as chosen by Franke [5] and used also by Kato and Launder [1] (see Figures 2 and 3). Accordingly an inflow value of $r_\mu = 100$ was taken.

In Table I, the present results are compared with those of Kato and Launder [7] obtained with wall functions (WF), using the standard $k-\varepsilon$ model, and the modification proposed by Kato and Launder. In addition, a comparison is included with Franke's [5] results, using the two-layer (TL) approach with the standard $k-\varepsilon$ model. From the first four rows it can be seen that there is neither systematic nor significant deviation from the results of Kato and Launder with either turbulence model; the difference in the force coefficients and the Strouhal number is smaller than the uncertainty of their evaluation.

Franke obtained a steady solution with the standard k–ε model in combination with wall functions, while in the present study with this combination, vortex shedding was observed. In the last two rows of Table I the results of Franke and of the present study are shown for the standard k–ε model, when used together with the one-equation model of Norris and Reynolds [12] in a two-layer approach. Again no systematic deviation of the results was found.

The conclusion from Table I is that when the same computational domain, boundary conditions and turbulence model are used, the different computer programs employed by Franke, Kato and Launder, and the present authors yield the same results.

3.2. Influence of inflow location and inlet conditions

The results reported in the previous section still depend on the inlet location and the inlet condition. Based on an estimate of the turbulent length scale, the value of r_μ, at the inlet in the simulations should be reduced. If instead of $r_\mu = 100$, as in the previous section, a value of $r_\mu = 10$ is specified at $x_{\text{inlet}}/D = -4.5$, the predicted drag coefficient $\overline{c_D}$ improves significantly, even with the standard k–ε model in combination with wall functions (WF). Table II summarizes the influence of the inflow conditions; the reference results given already in Table I are shaded. Comparing the results in rows 1 and 2 with the experimental data shows the influence of r_μ, specified at $x/D = -4.5$. The reduction of r_μ, corresponding to an increase of the dissipation rate $\langle\varepsilon\rangle$ at the inlet, also increases the Strouhal number *Str*.

The inlet conditions should be specified far enough in front of the cylinder, so that the calculated flow is independent of the location where the uniform inlet conditions are prescribed. The influence of the inlet location can be seen in Table II when the results with the WF standard k–ε model of rows 2 and 3 are compared. The results in row 2 were obtained with an inlet specified at $x_{\text{inlet}}/D = -4.5$ and in row 3 at $x_{\text{inlet}}/D = -10$. There is a strong influence also of the inlet location on the drag coefficient $\overline{c_D}$ and a weaker one on the Strouhal number *Str*. The comparison between rows 3, 4 and 5 shows that the results are still very sensitive to the specified value of r_μ for the inlet at $x/D = -10$.

If the influence of the boundary condition of $\langle\varepsilon\rangle$, specified through r_μ, and of the boundary condition location are considered simultaneously, the changes of $\overline{c_D}$ and *Str* by comparing rows 1 and 3 are smaller than the separate changes, because both effects partially compensate each other. Comparing row 6 and 7 for the Kato and Launder modification, together with wall functions and row 8 and 9 for the two-layer approach (TL) using the standard k–ε model, the

Table II. Force coefficients and Strouhal numbers dependence on the boundary conditions

Row		Turbulence model	x_{inlet}/D	r_μ	$\overline{c_D}$	c'_D	c'_L	*Str*
1	WF	Standard k–ε model	−4.5	100	1.618	0.0003	0.050	0.126
2	WF	Standard k–ε model	−4.5	10	1.834	0.0057	0.403	0.140
3	WF	Standard k–ε model	−10	10	1.637	0.0020	0.305	0.134
4	WF	Standard k–ε model	−10	5	1.697	0.0044	0.402	0.138
5	WF	Standard k–ε model	−10	20	1.555	0.0010	0.179	0.129
6	WF	Kato and Launder model	−4.5	100	2.108	0.0325	1.012	0.146
7	WF	Kato and Launder model	−10	10	1.789	0.0125	0.614	0.142
8	TL	Standard k–ε model	−4.5	100	1.750	0.0012	0.178	0.122
9	TL	Standard k–ε model	−10	10	1.719	0.0046	0.426	0.137
Experiments, see Table III					2.05–2.19			0.135–0.139

Table III. Force coefficients and Strouhal numbers dependence on the turbulence modeling and results of experiments

Near-body treatment	Far-body treatment	$\overline{c_D}$	c'_D	c'_L	Str
WF	Standard $k-\varepsilon$ model	1.637	0.0020	0.305	0.134
WF	Kato and Launder model	1.789	0.0125	0.614	0.142
TL	Standard $k-\varepsilon$ model	1.719	0.0046	0.426	0.137
TL	Kato and Launder model	2.004	0.0683	1.175	0.143

Experiments	Re	Tu (%)		
[30]	176 000	≈ 3	2.05	0.126
[25]	$\approx 50\,000$	< 1.2	2.19	0.123
[1]	22 000	2		0.135
[28]	14 000	6		0.139

change in the results can be seen when the improved boundary conditions are used. Using the WF standard $k-\varepsilon$ model, $\overline{c_D}$ and Str improve (rows 1 and 3), but with the TL standard $k-\varepsilon$ model and the WF Kato and Launder modification, the drag coefficient $\overline{c_D}$ gets worse and the Strouhal number Str improves.

3.3. Discussion of the results

In this section, the results are presented only with the optimized inlet location and conditions ($x_{inlet}/D = -10$ and $r_\mu = 10$). If a comparison with numerical results of other authors is made, it should be keep in mind that the boundary conditions are different so that the results can be compared only partly.

Table III summarizes the computed components of the force coefficients and the non-dimensional vortex-shedding frequency Str, and compares them with experimental results of different authors. For the near-wall region either the wall functions (WF) or the two-layer model (TL) is used. Away from the cylinder, either the standard $k-\varepsilon$ model or the modification proposed by Kato and Launder [1] is used. Using the wall function approach, the mean and fluctuating parts of both force coefficients increase when the standard $k-\varepsilon$ model is replaced by the modification of Kato and Launder. The increase of the fluctuating parts is caused by the stronger vortex shedding, observed with the Kato and Launder modification and thus $\bar{c}_D$ improves compared with the experiments. It should be noted that with the Kato and Launder modification, Str becomes slightly larger than in the experiments.

The same tendency can be seen, when the two-layer approach (TL) is used. Again with the Kato and Launder modification the force components and the Strouhal number increase. The improved results obtained with the Kato and Launder modification in a two-layer approach are as good as the results with the full Reynolds stress model reported by Franke [5].

In Figure 5 the distribution of the non-dimensional vorticity $\langle\omega_z\rangle D/u_\infty$ (with the vorticity $\langle\omega_z\rangle = \partial\langle v\rangle/\partial x - \partial\langle u\rangle/\partial y$) in the vicinity of the cylinder is shown for the different turbulence models. The different cases are not at the same phase angle, which should be noted when comparing the results. It can be seen that, with the improvement of the near-wall treatment and the use of the modification of Kato and Launder, the vortices starting at the leading edges of the cylinder get stronger and roll-up more into the wake of the cylinder. The standard $k-\varepsilon$ model with wall functions exhibits very long-stretched vortices. Independent of the near-wall

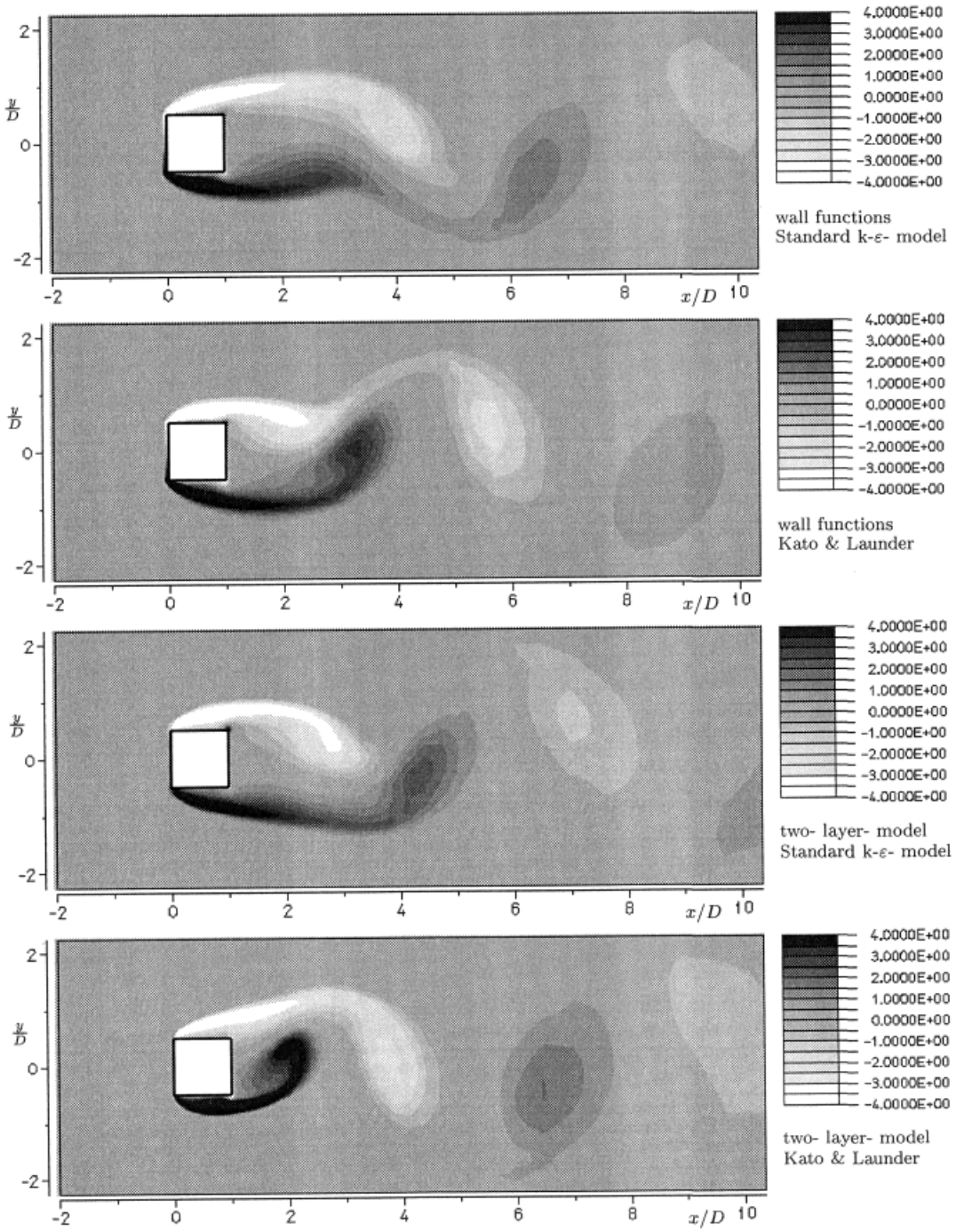

Figure 5. Calculated distribution of the vorticity $\langle \omega_z \rangle D/u_\infty$ with different turbulence models.

treatment, the centers of the separated vortices stay on their side with respect to the cylinder centerline. When the modification of Kato and Launder is used, the centers of the vortices cross over into the other half-plane, as observed in the flow visualization of Bearman and Trueman [25]. The instantaneous vorticity pictures show clearly that the peak vorticity increases when the standard k–ε model is replaced by the modification of Kato and Launder, and the wall functions are replaced by the two-layer model.

In Figure 6, contours of the time mean, non-dimensional turbulent kinetic energy $\bar{k}/u_\infty^2$ are shown in the surroundings of the cylinder. Comparing the different cases shown in this figure, it is obvious that the global behaviour of $\bar{k}$ is determined by the turbulence model used far away from the cylinder. In front of the cylinder, the increase of the turbulent kinetic energy can be see in both cases with the standard k–ε model, and this increase is significant for the flow behaviour in the wake of the cylinder.

In Figure 7 the distribution of the time mean turbulent kinetic energy $\bar{k}/u_\infty^2$ on the symmetry line at $y = 0$ is shown as obtained with the different turbulence models. In this plot, the measured distribution of Lyn *et al.* and the calculation results of Franke using the full Reynolds stress model and the standard k–ε model in a two-layer approach are shown. All the calculations can be seen to lie considerably below the experimental results. The Reynolds stress model, although a higher-order turbulence model, does not show any superior behaviour.

The results of this figure can be extracted also from Figure 6 and it can be seen that at the symmetry line the turbulent kinetic energy is smaller than in the surroundings of the symmetry line. To estimate the variation of $\bar{k}$, the peak values found in the wake behind the cylinder can be used as characteristic values. Table IV gives the maximum values of the non-dimensional turbulent kinetic energy, found downstream of the cylinder. Also in this table, the locations x/D and y/D of the maxima are given; the x-location is correlated with the length of the recirculation zone. Firstly, the maximum values of $\bar{k}/u_\infty^2$ differ significantly for the different models. With the standard k–ε model, independent of the near-wall treatment, higher values are observed in the wake. This is caused by higher levels in front of the cylinder. The near-wall treatment does not show any unique behaviour: replacing the wall functions by the two-layer approach yields the standard k–ε model higher values, while for the Kato and Launder modification it yields smaller maximum values in the wake. A single maximum occurs in the case of the Kato and Launder modification with the two-layer approach on the symmetry line, while in all other cases the maxima occur off the symmetry line. In these cases, a different roll-up process of the vortices behind the cylinder might cause increased levels of $\bar{k}/u_\infty^2$ on the symmetry line.

Lyn [26] presented a time trace of the pressure recorded on the side of the cylinder, which shows a variation between the different vortex-shedding periods. This variation might be interpreted as a low-frequency modulation of the vortex shedding and may originate from the 3D nature of the large scale structures. In the measurements, this contributes to $\bar{k}$ because it is not correlated with the phase angle. In his 3D large eddy simulations, Pourquié (private communication) observed a similar variation as shown by Rodi [27]. His calculated $\bar{k}$ on the centerline agrees well with Lyn *et al.*'s measurements, which may explain the failure of the statistical models there because the 2D calculations cannot capture the 3D nature of large-scale fluctuations.

Figure 8 shows the distribution of the non-dimensional velocity component $\bar{u}/u_\infty$ and Figure 9 of the non-dimensional total fluctuating energy $\bar{k}_f/u_\infty^2$ on the cylinder center line. The total fluctuating energy comprises the turbulent and the periodic fluctuations, and this quantity is free from any systematic error introduced in the phase-averaging data evaluation procedure in the experiments. In addition to the experimental results of Lyn *et al.* [2] and Durao *et al.* [28], the calculated distributions of Franke [5] and of the present study are included.

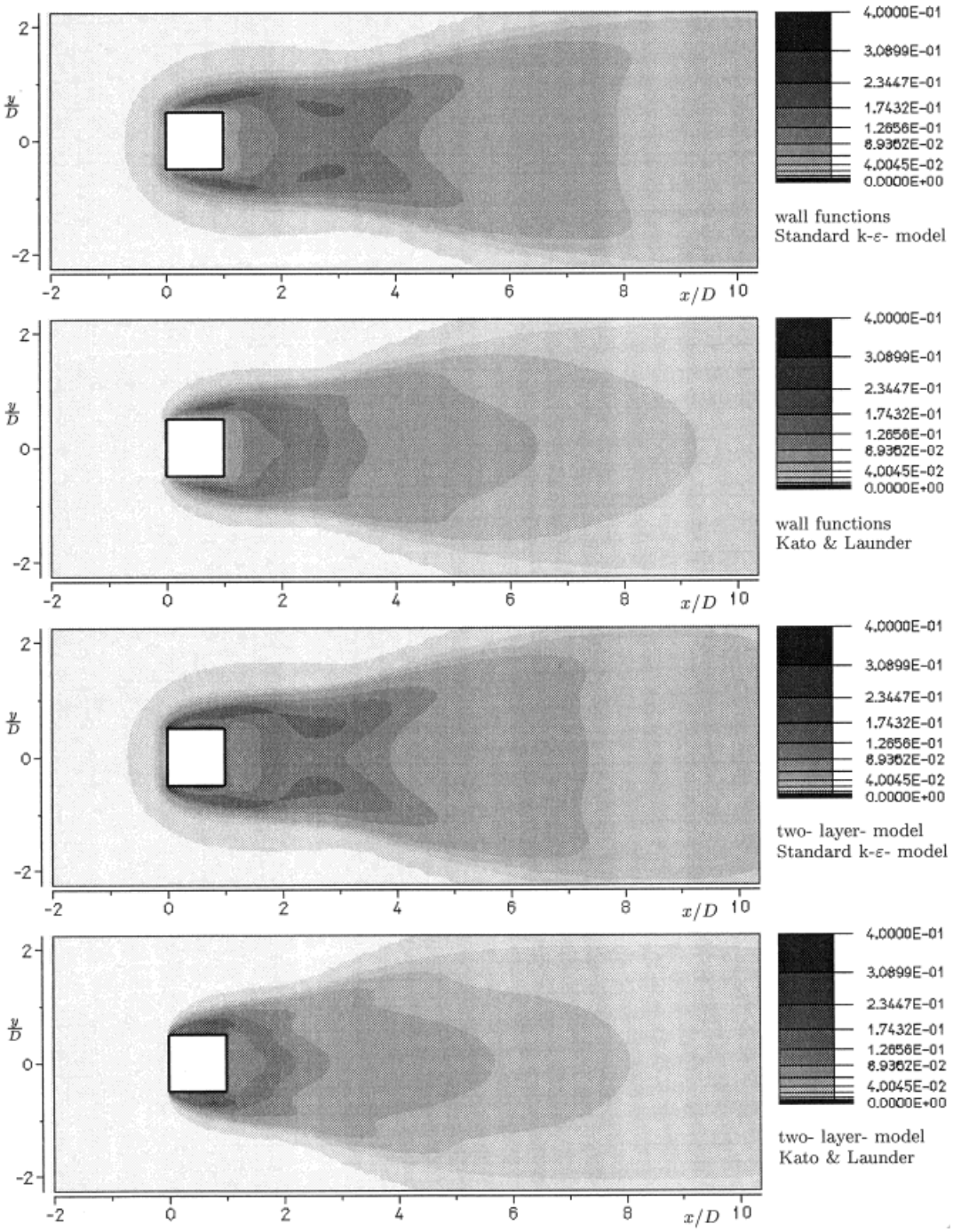

Figure 6. Calculated distribution of the turbulent kinetic energy $\bar{k}/u_\infty^2$ with different turbulence models.

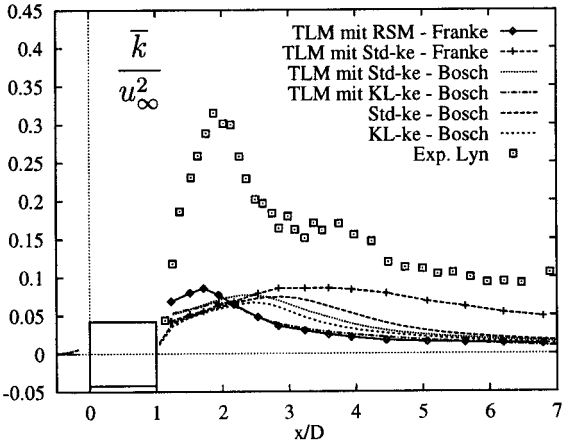

Figure 7. $\bar{k}$ on the symmetry line of the cylinder.

Table IV. Maximum levels of $\bar{k}/u_\infty^2$ in the wake of the cylinder

	Turbulence model	x/D	y/D	$\bar{k}/u_\infty^2$
WF	Standard k–ε model	2.4	0.70	0.091
WF	Modification of Kato and Launder	2.1	0.50	0.080
TL	Standard k–ε model	2.4	0.55	0.095
TL	Modification of Kato and Launder	1.9	0.00	0.068

The distributions in Figure 8 determined with the standard k–ε model, irrespective of the treatment close to the cylinder, indicate a recirculation zone which is too long. Using the two-layer approach instead of wall functions reduces the length of the recirculation zone. Considerable improvement is obtained with the Kato and Launder modification, especially when it is combined with a two-layer approach. The results are even superior to those obtained by Franke with the much more complex Reynolds stress model. However, they still approach the free-stream velocity faster than Lyn *et al.*'s experiments. Here, the agreement is comparable

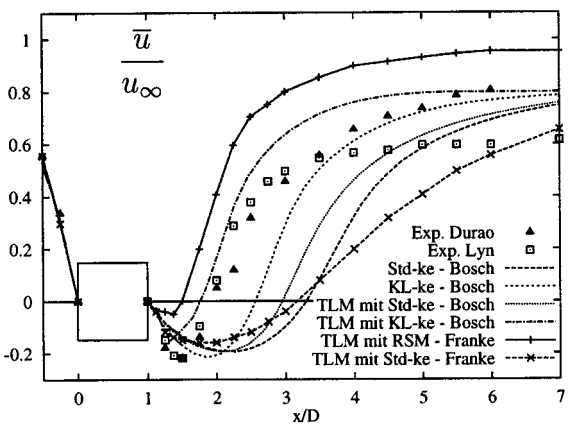

Figure 8. $\bar{u}$ on the symmetry line of the cylinder.

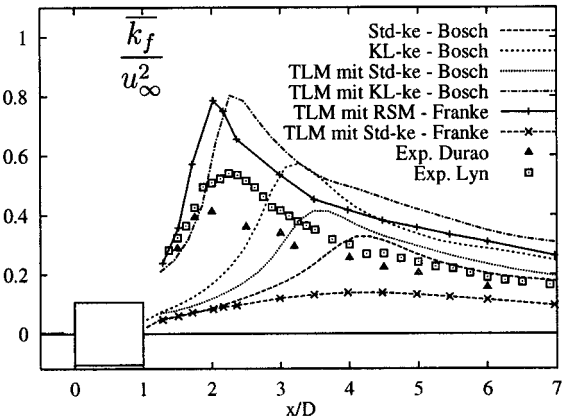

Figure 9. $\overline{k_f}$ on the symmetry line of the cylinder.

with Durao *et al.*'s measurements, but these were conducted with a different blockage and free-stream turbulence level (see Table III).

The total fluctuating energy $\overline{k_f}$, shown in Figure 9, is determined to be too low if the standard k–ε model is used. This is due to the overproduction of turbulent kinetic energy in front of the cylinder, resulting in a too strong damping of the periodic shedding motion in the wake of the cylinder. When the Kato and Launder modification is applied together with the two-layer approach, $\overline{k_f}$ is overpredicted, similar to the results of Franke obtained with a Reynolds stress model. Hence, with these turbulence modeling approaches, an overly strong periodic shedding seems to be produced, leading to time-averaged recirculation zone which is too short, as can be seen in Figure 8. It should be mentioned that with these modeling approaches, the location of the total fluctuation maximum in Figure 9 is determined correctly. If instead of the two-layer approach, wall functions are used together with the Kato and Launder modification, the maximum values are predicted correctly but the peak is shifted downstream compared with the experiments.

4. CONCLUSIONS

Good agreement was obtained with the simulations performed by Kato and Launder [1] and Franke [5] when the same computation domain and boundary conditions were used, except for the case of the standard k–ε model with wall functions. In this case, Franke did not obtain any unsteady vortex shedding, while the calculations reported here and by other authors yielded shedding. It appears that the onset of vortex shedding is strongly influenced by the numerical details of the solution procedure. Once vortex shedding is established, these numerical details seems to be less important for the calculations, as the comparison of the various results has shown.

The calculation domain and boundary conditions chosen by Franke and used in other studies were found not to be optimal for a comparison with the experiments of Lyn *et al.*, because the inlet conditions are specified too close to the cylinder and the turbulent length scale of the oncoming flow chosen was too large. This study has shown that the choice of the inflow location and the inflow conditions have a significant influence on the calculation results; in future calculations the optimized conditions proposed here should be adopted.

The main part of the paper dealt with the influence of the turbulence model employed on the prediction of the vortex-shedding flow past a square cylinder. Irrespective of the near-wall treatment used, it was found that the Kato–Launder modification produced superior results to the standard k–ε model. Due to the much reduced turbulence production in front of the cylinder, less turbulence is swept around the corners and the vortices roll in much stronger and even cross the symmetry line. Concerning the turbulent kinetic energy predictions, it was found that there is a significant underprediction by the statistical turbulence models compared with the experimental data and LES calculations. A reason for this may be the low-frequency modulation of the vortex shedding found in the experiments and in the LES simulations. This is counted as turbulence and cannot occur in 2D calculations. Concerning the velocity distribution on the center-line, it can be concluded that the use of the two-layer approach instead of the wall functions, or the Kato–Launder modification instead of the standard k–ε model improve the agreement with the measurements, also concerning the length of the recirculation zone. While the other models overpredict the recirculation length due to the underprediction of the periodic shedding motion, the Kato–Launder modification in combination with the two-layer approach underpredicts this length somewhat, but not as much as the full Reynolds stress model used by Franke. However, this model combination overpredicts the peak value of the total fluctuating energy $\bar{k}_f$, so that in view of the predictions of the turbulent energy, the periodic component must be overpredicted. A similar behaviour was obtained with the Reynolds stress model by Franke, but both models predict the correct location of the peak. Conversely, the correct level is predicted by the Kato–Launder modification in combination with wall functions, but the location is too far downstream.

The study has shown that the main quantities of engineering interest can be predicted reasonably well with k–ε type models. The use of the Kato–Launder modification has brought a major improvement, which was confirmed also by companion calculations of the flow around a square cylinder placed near a wall [29]. The best results were obtained when the Kato–Launder modification is combined with the two-layer approach. Not all the details of the complex motion are, however, in good agreement with the experimental observations. This is not very surprising in view of the presence of larger scale 3D fluctuations which lead to a low-frequency modulation of the shedding. These fluctuations cannot be accounted for in a 2D calculation approach, but only in a much more expensive 3D large eddy simulation.

ACKNOWLEDGMENTS

The work reported here was sponsored by the Deutsche Forschungsgemeinschaft through the Sonderforschungsbereich 210. Parts of the calculations have been performed on the Siemens VP S 600 at the Rechenzentrum of the University of Karlsruhe.

REFERENCES

1. M. Kato and B.E. Launder, 'The modelling of turbulent flow around stationary and vibrating square cylinders', *Proc. 9th Symp. Turbulent Shear Flows*, Kyoto, 10-4-1 (1993).
2. D.A. Lyn, S. Einav, W. Rodi and J.-H. Park, 'A laser-doppler velocimetry study of ensemble-averaged characteristics of the turbulent near wake of a square cylinder', *J. Fluid Mech.*, **304**, 285–319 (1995).
3. D. Laurence and J.-D. Mattei, 'Current state of computational bluff body aerodynamics', *J. Wind Eng. Ind. Aerod.*, **49**, 23–44 (1993).
4. V. Haroutunian, 'Progress in simulating industrial flows using two-equation models: can more be achieved with further research', *Industry-Wide Workshop on Computational Turbulence Modeling*, Ohio Aerospace Institute, October, 1994.

5. R. Franke, 'Numerische Berechnung der Instationären Wirbelablösung hinter Zylindrischen Körpern', *Ph.D. Thesis*, Universität Karlsruhe, 1991.
6. R. Franke and W. Rodi, 'Calculation of vortex shedding past a square cylinder with various turbulence models', in F. Durst *et al.* (eds.), *Turbulent* Shear *Flows 8*, Springer, New York, 1993, pp. 189–204.
7. B.E. Launder, G.J. Reece and W. Rodi, 'Progress in the development of a Reynolds-stress turbulence closure', *J. Fluid Mech.*, **68**, 537–566 (1975).
8. V. Przulj and B.A. Younis, 'Some aspects of the prediction of turbulent vortex shedding', *FED-Vol.* 149, Separated *Flows*, ASME, 1993.
9. M. Breuer and M. Pourquié, 'First experiences with LES of flows past bluff bodies', in W. Rodi and G. Bergeles (eds.), *Engineering Turbulence Modelling and Experiments 3*, Elsevier, Amsterdam, 1996, pp. 177–186.
10. W. Rodi, J.H. Ferziger, M. Breuer and M. Pourquié, 'Status of large-eddy simulation: results of a workshop', to appear in *J. Fluids Eng.*, (1997).
11. G. Bosch, 'Simulation der turbulenten umströmung eines quadratischen zylinders bei $Re = 22000$', *Report SFB 210/T/103*, Universität Karlsrnhe, 1997.
12. H.L. Norris and W.C. Reynolds, 'Turbulent channel flow with their moving wavy boundary', Dept. Mech. Eng., *Report FM-10*, Stanford University, 1975.
13. S. Majumdar, W. Rodi and J. Zhu, 'Three-dimensional finite-volume method for incompressible flows with complex boundaries', *J. Fluids Eng.*, **114**, 496–503 (1992).
14. J.P. Van Doormal and G.D. Raithby, 'Enhancements of the SIMPLE method for predicting incompressible fluid flows', *Numer. Heat Transfer*, **7**, 147–163 (1984).
15. C.M. Rhie and W.L. Chow, 'A numerical study of the turbulent flow past an isolated airfoil with trailing edge separation', *AIAA J.*, **21**, 1525–1532 (1983).
16. P.J. Roache, *Computational Fluid Dynamics*, Hermosa, Albuquerque, 1977.
17. B.P. Leonard, 'A stable and accurate convective modelling procedure based on quadratic upstream interpolation', *Comp. Methods Appl. Mech. Eng.*, **19**, 59–98 (1979).
18. S.V. Patankar, *Numerical Heat Transfer and Fluid Flow*, McGraw-Hill, New York, 1980.
19. J. Zhu 'A low-diffusive and oscillation-free convection scheme', *Comm. Appl. Numer. Methods*, **7**, 225–232 (1991).
20. B.E. Launder and D.B. Spalding, 'The numerical computation of turbulent flow', *Comput. Methods Appl. Mech. Eng.*, **3**, 269 (1974).
21. W. Rodi, *Turbulence Models and their Application in Hydraulics*, 3rd edn., Balkema, Rotterdam, 1993.
22. D.B. Taulbee and L. Tran, 'Stagnation streamline turbulence', *AIAA J.*, **26**, 1011–1013 (1988).
23. J. Cordes, 'Entwicklung eines zwei-schichten-turbulenzmodells und seine anwendung auf abgelöste, zwei-dimensionale strömungen', *Ph.D. Thesis*, Universität Karlsruhe, 1992.
24. G. Bosch and D.A. Lyn, 'Sensitivity of turbulent vortex shedding simulations on the numerical conditions', in preparation (1997).
25. P.W. Bearman and D.M. Trueman, 'An investigation of the flow around rectangular cylinders', *Aeronaut. Q.*, **23**, 1–6 (1971).
26. D.A. Lyn, 'Ensemble-averaged measurements in the turbulent near wake of a square cylinder', Interimsreport, Purdue University, West Lafayette, 1992.
27. W. Rodi, 'Comparison of LES and RANS calculations of the flow around bluff bodies', to appear in *J. Wind Eng. Ind. Aerodyn.* (1997).
28. D.F.G. Durao, M.V. Heitor and J.C.F. Pereira, 'Measurements of turbulent and periodic flows around a square cross-section cylinder', *Exp. Fluids*, **6**, 298–304 (1984).
29. G. Bosch and W. Rodi, 'Simulation of vortex shedding past a square cylinder near a wall', *Int. J. Heat Fluid Flow*, **17**, 267–275 (1996).
30. B.E. Lee, The effect of turbukence on the surface pressure field of a square cylinder, *J. Fluid Mech.*, **69**, part 2, 263–282.

